Raman Spectroscopy Methods to Characterize the Mechanical Response of Soft Biomaterials

Hui Zhou, Chelsey S. Simmons, Malisa Sarntinoranont, and Ghatu Subhash[*]

Mechanical and Aerospace Engineering, University of Florida, Gainesville, Florida, 32611 USA

ABSTRACT

Raman spectroscopy has been used extensively to characterize the influence of mechanical deformation on microstructure changes in biomaterials. While traditional piezo-spectroscopy has been successful in assessing internal stresses of hard biomaterials by tracking prominent peak shifts, peak shifts due to applied loads are near or below the resolution limit of the spectrometer for soft biomaterials with moduli in the kilo- to mega-Pascal range. In this review, in addition to peak shifts, other spectral features (e.g., polarized intensity and intensity ratio) that provide quantitative assessments of microstructural orientation and secondary structure in soft biomaterials and their strain dependence are discussed. We provide specific examples for each method and classify sensitive Raman characteristic bands common across natural (e.g., soft tissue) and synthetic (e.g., polymeric scaffolds) soft biomaterials upon mechanical deformation. This review can provide guidance for researchers aiming to analyze micromechanics of soft tissues and engineered tissue constructs by Raman spectroscopy.

INTRODUCTION

The mechanical properties of tissues and engineered constructs have been extensively studied at various length scales[1]. The performance and functionality of these tissues and engineered constructs are controlled by the hierarchical organization of various biological constituents from amino acid chains, macromolecules, fibrils, to fibers[2,3]. Understanding the relationship between changes in microscopic structure and macroscopic mechanical response provides insight into biological function, and a clear understanding of the relationship between microstructure and mechanical response can also guide design of new biomaterials and enable monitoring of changes during biomaterial fabrication and deformation[4,5].

Due to its high spatial resolution, non-invasive monitoring, and minimal specimen processing, micro Raman spectroscopy (μRS) has been a valuable technique for monitoring biochemical and structural information in biomaterials. μRS is a subset of vibrational spectroscopy which uses monochromatic light to provide a structural fingerprint by which molecules can be identified due to a specific pattern of molecular vibrations.[6] A complementary technique that utilizes molecular vibrations is Fourier-transform infrared (FTIR) spectroscopy.[7] In contrast to FTIR spectroscopy, μRS can collect data from aqueous samples, as the Raman scatter from water is weak, making it suitable for studies on cells and tissues. Also, μRS has a finer spatial resolution than FTIR spectroscopy.[8] In this review, we mainly focus on μRS. μRS have been widely applied to characterization of diverse biomaterials, including native and engineered tissues.[9,10] The applications of μRS to assessment of tissues is typically based on biochemical composition analysis, including *ex vivo* characterization of tissue functionality,[11,12] disease progression,[13,14] and in vivo diagnostic measurements[15]. Although μRS has been traditionally used for quantifying

composition in the biomaterials, efforts to use this technique to investigate mechanical response of biomaterials have been growing. One popular method to analyze the mechanical response of biomaterials to applied load is Raman piezo-spectroscopy, which correlates the shift in a specific spectral peak position to the magnitude of applied or residual stress in the material[16]. Piezo-spectroscopy has been effectively used on hard biomaterials (e.g., bone and teeth) which exhibit detectable peak shifts to applied loads.[17–20] However, for soft biomaterials (with modulus < 1 GPa), peak shifts under applied loads are negligible[21,22]. Hence determination of local stress is not currently possible for soft biomaterials such as ligaments[23] or synthesized hydrogel scaffolds with low stiffness such as collagen or fibrin hydrogels. Because the sensitivities of Raman peaks associated with molecular vibrations to mechanical deformation, Raman piezo-spectroscopy cannot be applied uniformly across all biomaterials under mechanical deformation. Figure 1 compares observed peak shift sensitivity under mechanical stress to Young's modulus for various biomaterials that have been studied using μRS[19–39]. The dashed line indicates the limit of the piezo-spectroscopy below which peak shifts are not currently detectable. While local stress magnitude may not be determined in these low-stiffness biomaterials, μRS can still be effectively used to determine local structural changes in these materials after mechanical deformation. Here, we review different approaches to characterizing physical and mechanical properties of soft biomaterials using μRS. We highlight known relationships between structural changes that occur at the macromolecular level and the Raman spectral features that best capture these changes.

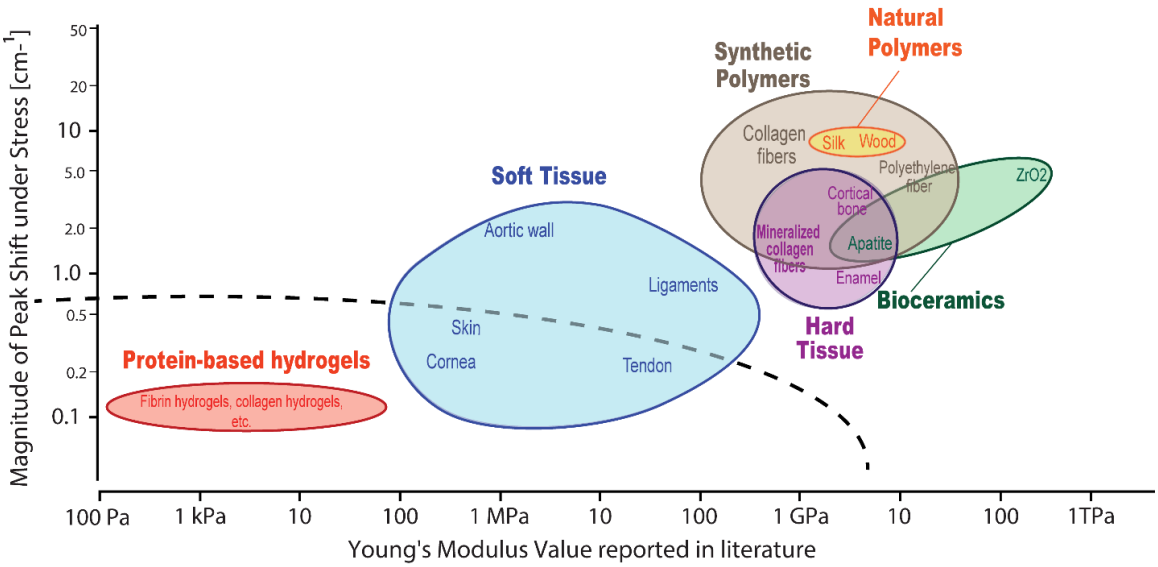

Figure 1. Biomaterials with sufficiently high moduli demonstrate quantifiable peak shifts while low modulus biomaterials exhibit peak shifts that are often below the measurement limit of μRS (represented by dash line). Data for this plot were compiled from references 10-30.

2. APPLICATION OF MICRO RAMAN SPECTROSCOPY TO BIOMATERIALS

2.1 Raman piezo-spectroscopy for hard biomaterials

Piezo-spectroscopy – from "piezo" in Greek meaning "to push" – is typically deployed to understand the mechanical properties of a material, i.e., the material's deformation in response to being "pushed". For soft biomaterials used in tissue engineering, an understanding of mechanical properties is helpful to evaluate fabrication parameters and to determine if the engineered construct can resist the mechanical forces anticipated after implantation. A simple test of mechanical properties is to apply a load in uniaxial tension or compression and measure the resulting deformation; after normalizing for the sample's cross-sectional area and original length, the slope

of this curve can be converted into a modulus (units: Pascals, Pa). While the determination of the macroscopic stress state in a mechanically loaded structure (i.e. applied load divided by the original cross-sectional area of the test sample) is common practice in experimental mechanics, most commonly used strain measurement methods (e.g., strain gages, photoelasticity, Moire interferometry, etc.) are not applicable for backing out the stress at the scale of material microstructure due to the unknown and complex relationship between the stress and strain. This task of stress quantification becomes more challenging if the microstructure is highly heterogeneous or hierarchical, such as those typically observed in biomaterials. Due to its high spatial resolution, μRS is ideally suited to detect microscale stress or strain distribution in such materials. High stiffness biomaterials such as calcified tissue (e.g., bone and teeth) and synthetic bioceramics which can withstand large stress levels show detectable Raman peak shifts upon deformation.[7] By calibrating the shift of a specific spectral peak to the applied stress, the piezo-spectroscopic coefficient, i.e. stress per wave number shift, is obtained as is commonly done for traditional engineering materials[17,40–46]. Pezzotti et al. studied the mechanical response of bone under four-point bending and determined a piezo-spectroscopic coefficient of 2.45cm^{-1}/GPa by tracking the spectral band of hydroxyapatite (nominally 980 cm^{-1}) as a function of the magnitude of applied stress (Fig. 2a-2b).[16] The 980 cm^{-1} band corresponds to the symmetrical stretching of the tetrahedron of oxygen atoms surrounding the phosphorous atom as indicated by the inset in Figure 2b and this Raman band is distinct from the spectrum of calcium phosphate ceramics. Knowledge of the piezo-spectroscopic coefficient enabled spatial mapping of microscale stresses for components of bone including calcified apatite and pre-calcified collagen (Fig. 2c). Apatite- and collagen-rich regions were differentiated based on the intensity ratio of hydroxyapatite (980 cm^{-1}) and collagen (2940 cm^{-1}) bands in the Raman spectrum. Under an applied macroscopic

flexural compressive stress of 40 MPa, high stress regions were found to correspond with calcified apatite-rich regions. Similarly, they characterized microscopic stress distribution at the interface between enamel (more rigid) and dentin (less rigid) in teeth by examining shifts of the hydroxyapatite band.[16] After determining a piezo-spectroscopic coefficient from hydroxyapatite band shifts under various macroscopic compressive stress magnitudes from 10 to 50 MPa, they observed that the enamel layer was mostly in tension while the dentin core was mostly in compression. Importantly, this study illuminated the complex load-bearing mechanisms of biological structures where soft and hard materials coexist with a stress-free interface.

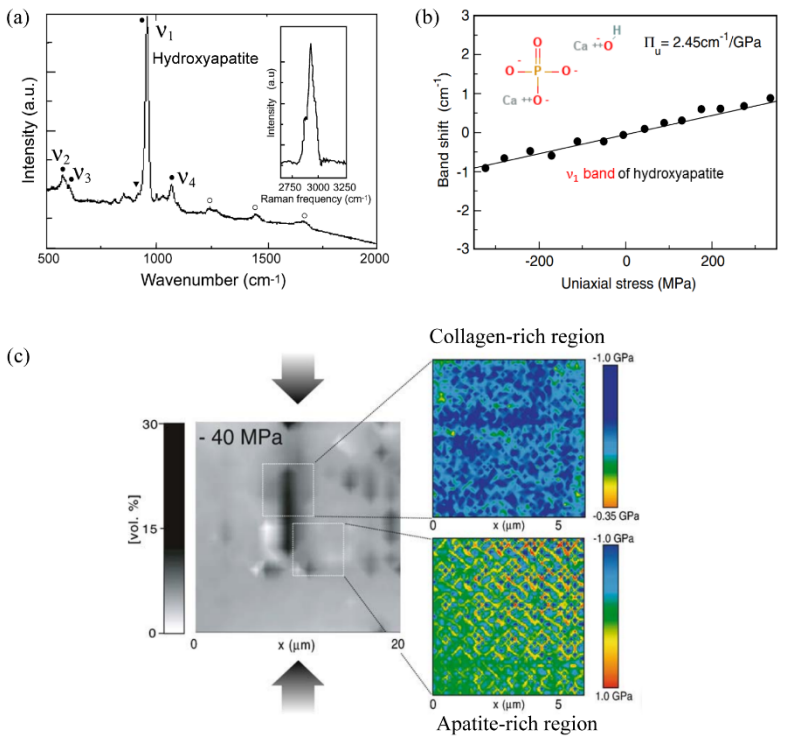

Figure 2. Local stress distribution determined by Raman piezo-spectroscopy indicates magnified compressive stress in collagen-rich phases and reduced stress in apatite-rich phases in cortical bone. (a) Hydroxyapatite peak ν_1 in bone used for piezospectroscopic calibration and collagen peak (inset) for volume calculation; (b) Evolution of Raman peak shift of hydroxyapatite band

(chemical structure inset) with magnitude of applied uniaxial stress; (c) Collagen volume fraction map (left) in cortical bone was determined by peak intensity ratio of hydroxyapatite (980 cm^{-1}) and collagen (2940 cm^{-1}). Inset maps show microscopic stress distribution calibrated by Raman piezo-spectroscopy in different regions, enabling correlation of collagen content with material properties. Adapted by permission from Springer Nature License: (Springer Nature) Analytical and Bioanalytical Chemistry (Raman piezo-spectroscopic analysis of natural and synthetic biomaterials, Giuseppe Pezzotti[16]), Copyright © 2004 Springer Nature.

Both cortical bone and teeth have highly mineralized apatite which has a high modulus in the range of 1-6 GPa.[47–49] Most soft tissues of the body do not have such high mineralized content and hence cannot sustain high stress levels needed to deform the chemical bond and change the state of the bond vibration. While soft biomaterials exhibit large macroscopic strain (deformation), the stress required to cause the molecular conformational changes is very small, and hence the Raman peak shift is below the detection limit of the piezo Raman method. Therefore, without a detectable peak shift, the Raman piezospectroscopic method cannot be applied in these soft tissues. To illustrate the importance of mineralized content in biomaterials for piezo-spectroscopic analysis, Chatzipanagis et al.[22] synthesized mineralized collagen fibers by uniformly distributing nano-apatite crystals in a collagen matrix and generated physical features similar to those found in newly formed bone tissue. By changing the volume fraction of these mineralized nanocrystals, the Young's modulus of collagen fibers was varied from 0.5 to 6 GPa. Shifts in the phosphate-related proline band (nominally 855cm^{-1} assigned to a carbon-carbon stretching or carbon-carbon-hydron bending) in the mineralized micro-fiber were monitored under uniaxial tension. While there were obvious peak shifts for mineralized collagen fibers with high modulus, no detectable peak shift was observed for non-mineralized collagen fibers with sub-GPa modulus (Figure 3a). This

experiment further confirms that soft biological tissue without mineralized content cannot sustain large stress and cannot exhibit detectable peak shift. Therefore, these materials cannot be probed using piezospectroscopic analysis.

Furthermore, within our own group, we determined that piezo-spectroscopy is not suitable for non-mineralized collagen-based biomaterials after examining three common hydrogels: naturally derived type I collagen, polyacrylamide, and polydimethylsiloxane. Even for large deformations of up to 100% strain, Raman peak-shifts of these hydrogel backbones could not be observed (Fig. 3b). It is likely that the polymer chains uncoil or slide past each other without sustaining enough stress to deform bonds. Hence, there is no measurable change in their vibrational frequency. However, understanding the mechanical response of natural (e.g., soft tissue) and synthetic (e.g., scaffolds) biomaterials at the microscopic level to applied deformation is of great importance to regenerative medicine and the ability to engineer tissue surrogates that withstand physiological loads. Despite its critical role in design of tissue constructs, there are few experimentally validated studies linking applied deformation to microstructural changes in soft biomaterials. In the following sections, we summarize various Raman spectral features that have been previously utilized to understand the response of a range of soft biomaterials to applied mechanical forces. We also provide suggestions for new analyses methods to further improve the utility of Raman spectroscopy for deciphering the soft tissue response.

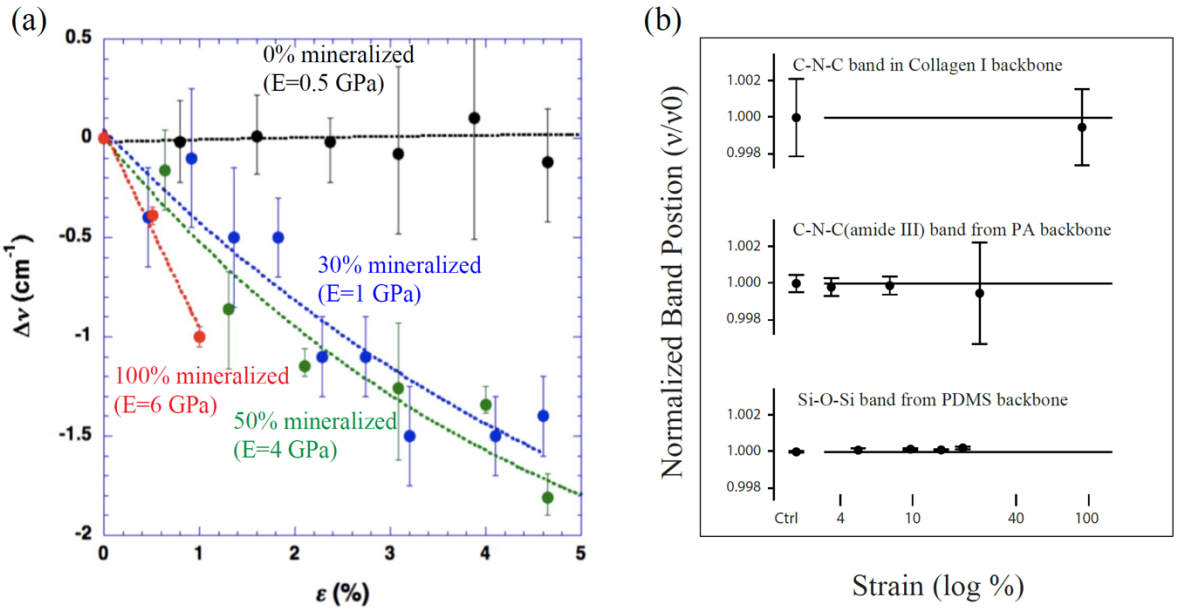

Figure 3. (a) Raman peak shift of the proline band increased in mineralized collagen fibers under uniaxial strain. No peak shift was detected for unmineralized collagen while a higher degree of mineralization yielded higher piezocoefficients (0% (black), 30% (blue), 50% (green) and 70% (red) mineral content of the micro-fibers). "In Situ Mechanical and Molecular Investigations of Collagen/Apatite Biomimetic Composites Combining Raman Spectroscopy and Stress-Strain Analysis" by Chatzipanagis et al.[22] is licensed by under CC BY 4.0. (b). Band position of the backbone bond normalized to band position at 0% strain for naturally derived type I collagen, polyacrylamide (PA) and polydimethylsiloxane (PDMS) as a function of uniaxial tension strain. (Data from authors' work)

2.2 Polarized Raman spectroscopy applied to soft biomaterials with ordered structures

Soft biomaterials contain highly ordered hierarchical structures, for example protein chains in a biological tissue. Polarized Raman spectroscopy can be effectively used to provide information on the molecular chain orientation. In polarized Raman spectroscopy, incident and collected

(scattered) light are defined by electromagnetic vectors (Fig. 4). For vibrations along these vectors, the measured intensities are higher compared to those when the vibrations are perpendicular to the vectors. In ordered biological tissues with aligned microstructural units, one anticipates highest Raman intensity when aligning the polarized incident and collected light with the biomaterial's axis of alignment (i.e. the XX configuration show in Fig. 4). The same principle is also used in polarized fluorescence[50] where structural features such as the orientation of fluorescent molecules, can be selectively recorded.[51] Förster resonance energy transfer can also provide structural information of biomaterials, such as the conformation of proteins. However, these imaging modalities are limited to the incorporation of exogenous fluorescing constructs. The application of polarized Raman spectroscopy allows for a label-free characterization of molecular orientations and conformation of the molecules in the sample. [9]

Table 1 summarizes previously reported results for three widely investigated biomacromolecules (collagen, elastin and fibroin) and their corresponding polarization-sensitive Raman bands under mechanical deformation. To describe the polarized measurements, Porto notation[52] is used to indicate a sample's axis of alignment with respect to the incident and scattered light polarization (Fig. 4). Differences in intensities of the Raman bands in the different polarization configurations show the preferential orientations of vibrations with respect to the microstructural units investigated. Hence, leveraging these sensitive Raman bands, polarized Raman measurements with respect to the biomaterials' axis of alignment can be applied to determine orientation of the microstructure in the indicated biomaterials. Furthermore, the quantity of the polarized intensity (ratio) or polarized Raman band area (ratio) of certain sensitive band(s) is measured and correlated to mechanical deformation, indicating the alignment change of the structure in the soft biomaterials under mechanical deformation.

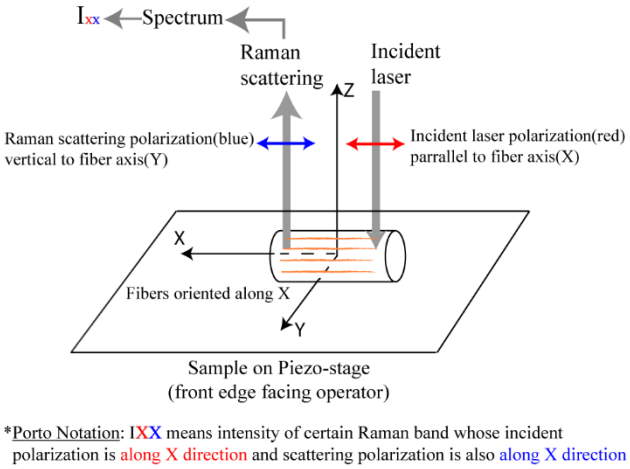

Figure 4. Schematic showing the alignment of Raman polarization axis with respect to fiber axis and the corresponding Porto notation for the oriented sample. Note, for example, the depicted setup is in the I_{xx} orientation[52].

Table 1. Raman bands sensitive to laser polarization and structure orientation for soft biomaterials

Macromolecule	**Raman band**	**Material**	**Intensity comparison at different polarization states**	**Preferential vibration orientation (∥, parallel; ⊥, perpendicular)**	**Reported Application in analysis associated with mechanical deformation**
Collagen	Amide-I C=O (β-sheet)	Rat tail tendon[21]	$I_{x\_} < I_{y\_}$; $I_{yy} > I_{xx}$	⊥ collagen fibrils	$\frac{I_{yy}(1665)}{I_{xx}(1665)}$ ↑ with tension
		Bovine tendon, human skin[53]	$I_{x\_} < I_{y\_}$		-
		Bovine tendon[54]	$I_{xx} < I_{xy}$		$\frac{I_{1245}}{I_{1268}}$ as a collagen orientation marker
		Rat tail tendon[55]	$I_{yy} > I_{xx}$; $I_{yy} > I_{xy}$		$\frac{I_{yy}-I_{yx}}{I_{yy}+2\times I_{yx}}$ ↑ a higher degree of collagen fiber alignment
	Amide-I C=O	Rat tail tendon[56]	$I_{x\_} > I_{y\_}$	∥ fascicle axis	-

	(α-helix)				
	Amide III N-H (ordered, helix)	Bovine tendon[53]	$I_{x\_} < I_{y\_}$	⊥ collagen fibrils	Amide III doublet ratio as a collagen orientation marker
		Bovine tendon[54]	$I_{xx} < I_{xy}$		-
		Human dermis[57]	$I_x < I_y$		-
		Aligned collagen thread[58]	$I_{xx} < I_{yy}$		Amide III doublet susceptible to polarization
	Amide III C-N (random coils)	Rat tail tendon[55]	I_{xx} (or $I_{xy\_}$) < I_{yy} (or I_{yx} or $I_{y\_}$)	∥ fascicle axis	$\frac{I_{xx}-I_{xy}}{I_{xx}+2\times I_{xy}}$ ↑ a higher degree of collagen fiber alignment
		Aligned collagen thread[58]	$I_{xx} > I_{yy}$		I_{1245}/I_{1454} susceptible to fibril orientation
	C–C skeletal	Rat tail tendon[55]	I_{xx} (or $I_{x\_}$) < I_{yy} (or I_{yx} or I_{xy})	∥ fascicle axis	$\frac{I_{xx}-I_{xy}}{I_{xx}+2\times I_{xy}}$ ↑ a higher degree of collagen fiber alignment
	CH_3-CH_2	Aligned collagen thread[58]	$I_{xx} < I_{yy}$	⊥ collagen fibrils	I_{1320}/I_{1454} susceptible to fibril orientation
	C-C protein backbone	Rat tail tendon[55]	I_{xx} (or $I_{x\_}$) < I_{yy} (or I_{yx} or I_{xy})	∥ fascicle axis	$\frac{I_{xx}-I_{xy}}{I_{xx}+2\times I_{xy}}$ ↑ a higher degree of collagen fiber alignment
		Bovine tendon[53]	$I_{x\_} > I_{y\_}$	∥ collagen fibrils	-
	ν(CCO)	Bovine tendon, human skin[53]	$I_{x\_} > I_{y\_}$	∥ collagen fibrils	-
	N-H protein backbone	Bovine tendon, human skin[42]	$I_{x\_} < I_{y\_}$	⊥ collagen fibrils	-
	Phenylalanine	Pig Cartilage[59]	$I_{xx} > I_{xy}$	∥ cartilage axis	-
	Pyranose ring	Pig Cartilage[59]	$I_{xx} > I_{xy}$	∥ cartilage axis	$I_{xx}(1126)$ ↓ after compression
Elastin	Phenylalanine	Bovine ligament[60]	$I_{xx} < I_{yy}$	⊥ fiber axis	$\frac{I_{xy}(860)}{I_{xx}(860)}$ ↑, $\frac{I_{yx}(860)}{I_{yy}(860)}$ ↓ with tension
	Amide I water	Bovine ligament[60]	$I_{xx} < I_{yy}$	⊥ fiber axis	$\frac{I_{xy}(1630)}{I_{xx}(1630)}$ ↑, $\frac{I_{yx}(1630)}{I_{yy}(1630)}$ ↓ with tension
Fibroin	Amide III N-H	Silk filament[61]	$I_{xx} > I_{yy}$	∥ fiber axis	$\frac{I_{xx}(1230)}{I_{xx}(1660)}$ ↓ with tension
		Spider[62–64]	$I_{xx} > I_{yy}$; $I_{xx} > I_{yx}$; $I_{xx} > I_{xy}$		$\left(\frac{I_{yy}(1668)\times I_{xx}(1228)}{I_{xx}(1668)\times I_{yy}(1228)}\right)^2$ ↑ with alignment
	Amide I C=O (β-sheet)	Silk monofilament[37]	$I_{xx} > I_{xy}$	⊥ fiber axis	$\frac{I_{xx}(1230)}{I_{xx}(1660)}$ ↓ with tension
		Silk filament[61]	$I_{xx} < I_{yy}$		-
		Spider[62–64]	$I_{yy} > I_{xx} > I_{yx}$(or I_{xy});		-

		Silk[65]	$I_{xx} > I_{xy}$		$\frac{I_{xy}(1667)}{I_{xx}(1667)} \uparrow, \frac{I_{xy}(1667)}{I_{xx}(1667)} \downarrow$ with tension

Polarized Raman spectroscopy can detect orientation changes of fibers within a soft tissue under mechanical deformation, e.g., changes in the orientation of collagen fibrils in tendon[21] and skin as it is stretched[53]. In many biological tissues, collagen structure is hierarchical and consists of collagen molecules assembled into fibrils, which are then bundled to form fibers. Each collagen fiber consists of protein segments within which a specific vibrational mode has been identified that is perpendicular to the backbone axis of the peptide. This C=O stretching mode of amide I corresponds to the 1668 cm^{-1} band in the Raman spectrum[66–68] and shows enhanced intensity when the polarization axis is 90° to the fibril axis (indicated by the blue line in Fig. 5a). This intensity information can be used to estimate the degree of fiber alignment at a given location in a rat-tail tendon. Masic et al. modeled intensity data as a cosine function and plotted the approximate fiber axis (Fig. 5b).[21] Fibers were initially aligned at approximately ± 30° to the tendon axis (Fig. 5b), and polarized Raman spectroscopy enabled real-time monitoring of fiber realignment along the direction of applied tensile load (insets in the stress-strain diagram, Fig. 5c).[21]

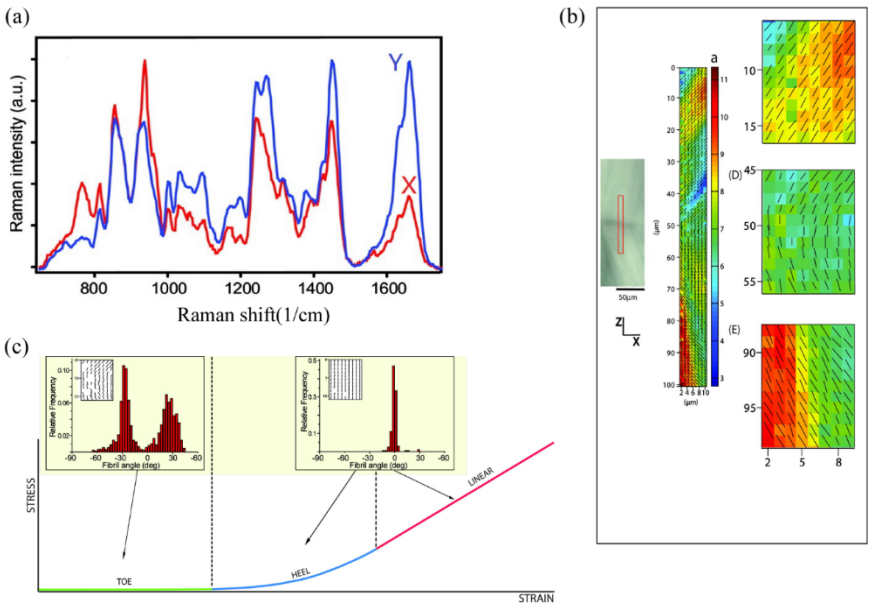

Figure 5. Application of polarized Raman spectroscopy to detect orientation of collagen fibers in a rat-tail tendon in undeformed and deformed states. (a) Raman spectrum of collagen in tendon in different polarization configurations shows higher intensity in YY polarization (blue, 90 degree) than XX polarization (red, 0 degree). (b) (Left) Optical microscopy image of collagen region and (center) a corresponding collagen fibril orientation map based on Raman peak intensity ratio analysis; (right) magnified regions revealing differences in orientation characterized across the tissue. (c) Stress-strain response of rat tail tendon under uniaxial tensile deformation. Inset shows collagen orientation as characterized by Raman peak intensity ratio analysis with respect to tendon fiber axis. As strain increases, fibers align along the axis of the tail. Reprinted with permission from ref 21. Copyright © 2011 American Chemical Society

Polarized Raman spectroscopy has also been applied to determine molecular level orientation in soft biomaterials. For fibrous elastin from the bovine nuchal ligament, Green et al.[60] used the mathematical model developed by Rousseau et al.[61] to determine degree of alignment of certain

molecular units in elastin. For obtaining information about molecular orientation, the average values of the Legendre polynomial ⟨ P2 ⟩ and ⟨ P4 ⟩ can be determined by fitting the experimentally determined polarized Raman intensity of a certain Raman band at different polarization angles. The second and fourth order parameters, ⟨ P2 ⟩ and ⟨ P4 ⟩, are the first two coefficients of the Legendre polynomial expansion of the orientation distribution function, and the orientation distribution can be estimated from these parameters by calculating the most probable orientation function. Calculations on Legendre polynomial ⟨ P2 ⟩ and ⟨ P4 ⟩ from the polarized intensity ratios of Raman bands showed that, for strains up to 60%, orientation, β-turns, ordered helix, and unordered structural components did not re-orient. However, the phenylalanine and tyrosine chain within the hydrophobic domains (1006 cm^{-1}) in ligaments were found to re-orientate closer to the fiber axis (at 90 degrees) from 39 to 42 degrees, whereas the tyrosine within the cross-linking regions re-oriented closer to the fiber axis from 35 to 49 degrees. Similarly, by putting the values of order parameters ⟨ P2 ⟩ and ⟨ P4 ⟩ into the most probable orientation function, Masic et al. [21] observed a sharpening of the distribution associated with the collagen molecule unit (C=O bond) during uniaxial tension of the tendon. Again, reorganization at the molecular level in the tissue is evaluated through a distribution function that is in agreement with tissue level orientation changes, as shown in Fig. 5c. Sereda et al.,[69] also used this method for structural characterization of amyloid aggregation, which plays an important role in a wide variety of human diseases. Based on the most probable distribution of the peptide carbonyl group orientation in the insulin fibrils, they found carbonyl groups were well ordered and almost parallel to the fibril axis, diverging only 13±5° relative to the main axis of the fibrils.

Wang et al.[25] also used polarized Raman spectroscopy to study polymer orientation at the molecular level of poly-l-lactic acid (pLLA) under mechanical deformation. pLLA is a commonly

used acid for polymer-based bioresorbable scaffolds, e.g. as a resorbable vascular stent[25]. However, changes in microstructure with degradation and under mechanical deformation can result in loss of structural integrity. Therefore, continuous monitoring of its microstructural organization is important for its clinical performance. Using the 875 cm^{-1} band assigned to the C-COO stretch mode of the polymer backbone, Wang and coworkers[25] measured molecular chain orientation of pLLA relative to the specimen axis. As the polymer becomes preferentially aligned in one direction, there is stretch of the extended backbone in that direction that results in enhanced intensity of the incident polarized light in that same direction. They found I_{875} became stronger and this intensity was normalized to that of the 1452 cm^{-1} band (bending mode of CH_3) which was used as an internal standard before structural degradation. The Raman spectra of pLLA sheets before deformation and after being uniaxial stretched up to 100% strain, are shown in Fig. 6b and 6d, respectively. The intensity ratio of I_{875}/I_{1452} was higher along the XX polarization configuration after being stretched compared to that before stretched as shown in Fig. 6c. This implies that molecular chains in pLLA are now aligned more toward the stretching direction.

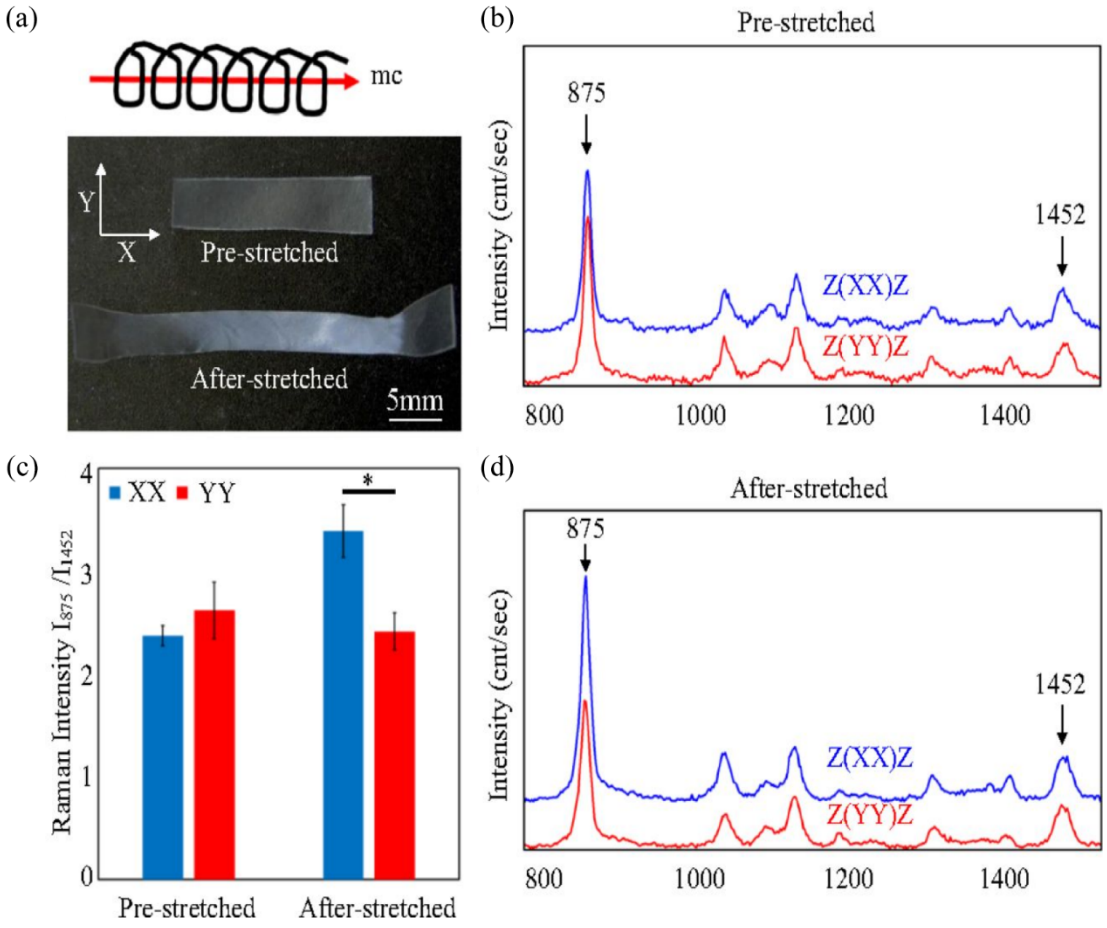

Figure 6. (a) Poly-l-lactic acid (pLLA) molecular chain axis (mc axis) and an image of the pLLA sheet before and after stretching. (b and d) Raman spectra of pLLA sheet before and after stretching for two polarization configurations (XX and YY). (c) Changes in intensity ratio of I_{875}/I_{1452} before stretching and after stretching shows that the intensity ratio at the XX polarization configuration becomes higher after being stretched in the X direction. "Strain-Induced Accelerated Asymmetric Spatial Degradation of Polymeric Vascular Scaffolds" by Wang et al.[25] is licensed by under PNAS license.

2.3 Raman spectroscopy for quantifying secondary structure in soft biomaterials

Protein in biological tissues assembles into primary, secondary and tertiary structures. For example, in fibrin proteins, the primary structure refers to a sequence of amino acids in a peptide chain. The peptide chains are held together by hydrogen bonds to form a secondary structure that can take several forms, such as α-helix, β-sheet, β-turn, and random coil. These secondary structures can further group together to form a tertiary structure in 3-dimensional folding patterns. μRS can be used to differentiate various forms of the secondary structure because each secondary structure corresponds to a different Raman band. The presence of a specific secondary structure of a protein can be quantified by calculating the area under the respective bands in the Raman spectrum. For example, μRS reveals that the secondary structure in fibrin hydrogels changes from α-helix to β-sheet upon mechanical deformation.[70] A broad amide I band in the Raman spectrum of fibrin was decomposed to different sub-bands with each representing certain secondary structure, such as α-helix, random coil and β-sheet. The relative volumes of secondary structures in fibrin are quantified by the area fraction of each sub-band relative to the total area of Amide I band. Fleissner et al.,[71] found that while the fraction of random coils remained the same, α helix content decreased and the fraction of β sheets increased when fibrin hydrogels underwent uniaxial tension. For up to 110% applied strain, the observed decrease in α helix content was the same as the observed increase in the quantity of β sheets, confirming the phase transition from α- helices to β-sheets in fibrin under tension. Further, the polarized Raman spectroscopy measurements reveal that the α helix band and the β sheet band remain isotropic in the virgin undeformed state but become anisotropic after deformation. β sheets tend to distribute in the direction 80 degrees to loading while α-helices mostly distribute along the loading direction, which can indicate the direction of the applied load. Hence, μRS on such secondary structures that respond to deformation

can further help in understanding of spatial heterogeneity and distributions of different microstructures in fibrin gels.

2.4 Deformation-sensitive Raman spectral features for soft biomaterials

The examples provided thus far highlight salient Raman spectral features that have been used to decipher changes in the microstructure of biological tissues when subjected to mechanical deformation. Taken together, biomaterial studies by μRS have identified specific spectral features that are sensitive to vibrational changes in certain functional groups when mechanical deformations are applied and can be grouped by corresponding mechanisms (Fig. 9). For example, certain amides show sensitivity to applied stress through a wave number change (peak shift) while others show only an intensity change under mechanical deformation. Thus, the anticipated concentration of relevant components in a soft biomaterial of interest, along with an estimate of its macroscale modulus, will inform which specific Raman spectral features are likely to yield the most helpful information and can guide experimental design using μRS for soft biomaterial characterization under mechanical deformation. Further details[72–91] of Raman bands information and their application for studying the responses of biomaterials under mechanical deformation are provided in Table S1 (supporting information).

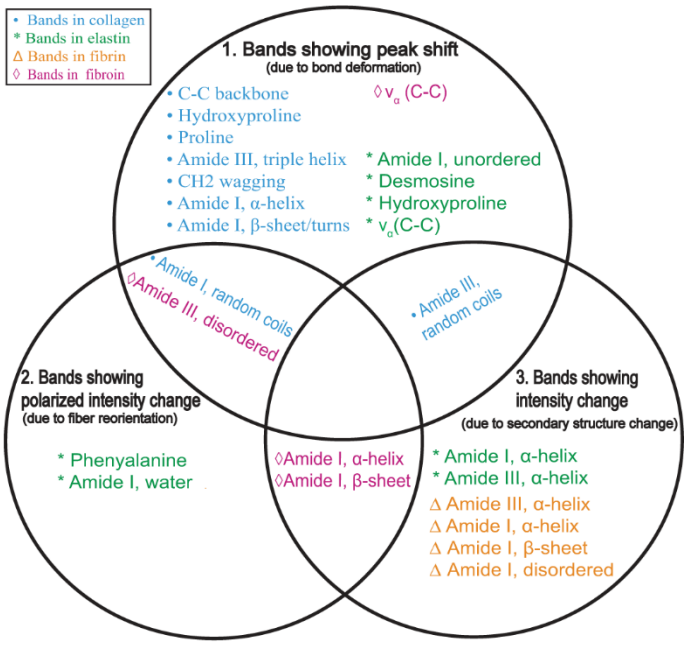

Figure 8. Raman bands in four protein-rich biostructures show different spectroscopic changes under mechanical deformation as demonstrated throughout the literature.[21–23,30,32–34,36,37,58,60,71,89,91]

3. CONLUSION AND FUTURE PERSPECTIVES

Although shifts in peak position are associated with piezo-spectroscopy of hard biomaterials, detectable peak shifts are not seen when Raman spectroscopy is applied to soft biomaterials. This review summarizes other Raman features that characterize microstructural changes within soft biomaterials under mechanical deformation. Specifically, intensity ratio of a given Raman band under different polarization orientations and intensity changes in the relevant peaks of secondary structure can be used to quantify microstructural evolution of soft biomaterials under deformation. Through calibration experiments, the quantity or the degree of alignment of microstructural components can be further correlated to strain or stress state of the biomaterial. Hence, by using

μRS coupled with an *in situ* mechanical loading apparatus, one can determine real-time, local changes in the mechanics of soft biomaterials non-destructively.

μRS thus offers the potential to characterize changes in local microstructure and quantify changes in living biomaterials due to applied mechanical deformation. Characterizing the mechanical response of soft tissues is important for understanding basic cellular function. Being able to monitor this response over time is critical to the field of regenerative medicine. In regenerative tissue engineering, most constructs undergo *in vitro* "maturation" while cells rearrange the microstructure, deposit additional matrix proteins, and differentiate into new cell types in an attempt to generate functional tissue. Due to its high spatial resolution, non-invasive monitoring, and minimal specimen preparation, Raman spectroscopy has been a valuable technique for assessment of tissue-engineered constructs.[92–95] For instance, Raman spectroscopy has been used to characterize the biomolecule distributions in the tissue-engineered articular cartilage[9] and to determine the viability of cells within oral mucosa-equivalent constructs.[92] However, few Raman spectroscopy studies have focused on changes in the mechanical response of tissue constructs, despite mechanical performance being a critical target. The mechanical response of engineered materials should mimic that of the human tissues they are aiming to replace, otherwise implants will fail. For example, tissue-engineered blood vessels often burst under normal physiological pressures,[96,97] which hinders clinical translation.[98]

In addition, biological cells used in tissue engineering are not passive filler materials but are 10-to-100 micrometer size elements that actively alter their surrounding matrix by contraction. Though small, traction forces at pico- or nano-Newtons per cell induce local deformation and residual stress on the matrix scaffold, so the effect of cell contraction can be large when compounded across centimeter-scale constructs. To accurately monitor the evolution of

mechanical properties in scaffolds due to cell contractility, a non-destructive, high-resolution tool like Raman spectroscopy offers substantial value over traditional techniques like traction force microscopy or fluorescing force probes that require introduction of additional materials.[99] However, the determination of such stress magnitude in soft biomaterials is non-trivial due to negligible peak shifts if only piezo-spectroscopy is adopted. μRS techniques that quantify changes in microstructural components and alignment need to be coupled to robust computational methods that predict stresses within scaffold structures. These approaches need to employ sophisticated constitutive models that account for stress distribution within hierarchical scaffold networks, e.g., cells, fibers and matrix components.[100]

Raman spectroscopy offers numerous advantages while characterizing biological tissues. It has the potential to determine not only biochemical organization but also mechanical organization of tissue constructs, e.g., organization of collagen fibers in rat tail tendon as shown in Fig. 5. Raman spectroscopic analysis can be performed *in situ* and does not require extensive sample preparation. It does not require contact with the sample as in atomic force microscopy, nanoindentation, and macroscale tensile testing. In addition, Raman spectroscopy affords non-invasive, label-free and real-time imaging of cell-laden scaffolds under normal physiological conditions in a way that many current imaging techniques cannot.[101] However, broad application of Raman spectroscopy to tissue-engineered scaffolds has limitations warranting further development.

One critical issue is the time it takes to acquire data. In conventional Raman spectroscopic analysis, the scanning time would be simply increased to ensure the quality of spectra. However, this is not always desirable for living biomaterials because the laser may heat the sample and cause unwarranted damage or changes in the cellular structure. Since Raman spectra are also prone to noise, reducing the noise to a level amenable with short acquisition time can be one way to deal

with negative side effects of long scan times. This may require use of noise reduction to enhance signal to noise ratio.[101] These methods include but are not limited to substrate selection such as nanomaterials and photonic structures to enhance the Raman signal,[102] increasing detector gain to obtain sufficient signals,[103] choosing non-linear optics to enhance Raman signal[104] and using fibre-optic Raman probes.[13] Another way to reduce scan time is by decreasing the total acquisition numbers or increasing the spatial scanning speed such that the total measured time for imaging a large area is reduced. The methods include but are not limited to choosing multimodal integration,[105] selective-sampling,[106] and projecting a laser line[107] or a multifocal scan[108] to obtain multiple spectra simultaneously.

Another common problem is the ambiguous interpretation of structural constituents when the spectra do not contain sharp peaks[109]. A broad band may contain substantial overlap of several peaks due to complex mixtures of constituents and spatial heterogeneity in soft biomaterials. These complexities demand new data analysis techniques for soft biomaterials. In recent years, multivariate approaches have emerged as a potential tool to analyze the data for complex biological materials.[110–113] A multivariate data set includes two variables referring to wavenumber and intensity. Each variable is treated as a dimension and thus multivariate matrix is used. As the Raman peak intensities change with each acquisition in time, location or other status (e.g., mechanical deformation), the analysis will reduce the number of dimensions and structures the data set in a way that clusters similar spectra and enhances the variance between different spectra. One such statistical method is principal component analysis (PCA) which is used to separate spectra based on the greatest variance with no *a priori* knowledge[114]. PCA has been used, often in combination with other statistical tools (e.g., various weighting methods), to discriminate between different biological samples[115,116]. While it is difficult to assign every spectral peak to individual

molecular species due to the complexity inherent to biological systems, use of biological databases[117–119] of Raman spectra coupled with systematic data analysis[120] could support further application of Raman to living biomaterials. Furthermore, the multivariate analysis can classify whether a sample belongs to a given group or not (e.g., whether it is healthy or diseased).[121,122] The results are reliable if the accuracy, sensitivity or specificity of the above classification meets a minimum threshold. For example, in clinical applications, the minimum threshold is usually set at 75%.[123] The classification procedure is iterative, and the user can go back and change the variables or the thresholds until convergence is achieved. First, the experimental dataset is split into two subsets- training set and testing set at a predetermined ratio (e.g., 80% to 20%). The mean and variance of the selected variables (e.g., peak positions) for each group is calculated in the training set and each data point in the testing set is assigned to the group based on proximity to the group mean normalized by the group variance. The testing set is then followed by a validation procedure to inform the accuracy of the assignment and assess the predictive classification ability. Thus, the confidence in the assignment is enhanced by acquiring a large data set which includes all the possible features of the sample space.

In summary, in addition to the Raman spectral peak sensitivity of biomaterials under mechanical loading to their modulus, we have described Raman sensitive features to microstructural changes in soft biomaterials under mechanical deformation: (i) polarized intensity change associated with alignment and (ii) intensity change associated with the quantity of secondary structures. However, these sensitivities of Raman bands do not shed light on the stress level induced in these biostructures. New analytical techniques, constitutive models, and computational models are needed to build the correlation between microstructural changes and stress or mechanical

properties of scaffolds so as to fully utilize the potential of Raman technique for non-invasive monitoring of the engineered tissue constructs.

ASSOCIATED CONTENT

Supporting Information. Raman bands information and their correlation to stress or strain for studying the responses of biomaterials under mechanical loading (Table S1), as mentioned in the manuscript.

AUTHOR INFORMATION

Corresponding Author

*Tel: +1 352 727 8662. Email: subhash@ufl.edu

ACKNOWLEDGMENTS

The authors acknowledge the support by the National Science Foundation under the grant CMMI-1762791 to the University of Florida. The authors also acknowledge the DoD-DURIP Instrumentation Grant "Acquisition of Upgrades for Raman Spectroscope for Enhanced Speed, UV and Polarization Capabilities" from ARO-68410-EG-RIP.

ABBREVIATION

Micro Raman spectroscopy (μRS)

REFERENCES

(1) Fratzl, P.; Weinkamer, R. Nature's Hierarchical Materials. *Prog. Mater. Sci.* **2007**, *52* (8), 1263–1334. https://doi.org/10.1016/j.pmatsci.2007.06.001.

(2) Shoulders, M. D.; Raines, R. T. Collagen Structure and Stability. *Annu. Rev. Biochem.*

2009, *78*, 929–958. https://doi.org/10.1146/annurev.biochem.77.032207.120833.COLLAGEN.

(3) Wang, A. Y.; Foss, C. A.; Leong, S.; Mo, X.; Pomper, M. G.; Yu, S. M. Spatio-Temporal Modification of Collagen Scaffolds Mediated by Triple Helical Propensity. *Biomacromolecules* **2008**, *9* (7), 1755–1763. https://doi.org/10.1021/bm701378k.

(4) Rehfeldt, F.; Engler, A. J.; Eckhardt, A.; Ahmed, F.; Discher, D. E. Cell Responses to the Mechanochemical Microenvironment-Implications for Regenerative Medicine and Drug Delivery. *Adv. Drug Delivery. Rev.* **2007**, *59* (13), 1329–1339. https://doi.org/10.1016/j.addr.2007.08.007.

(5) Samir, Mitragotri and Joerg, L. Physical Approaches to Biomaterial Design. *Nat. Mater.* **2009**, *8* (1), 15–237. https://doi.org/10.1038/jid.2014.371.

(6) Butler, H. J.; Ashton, L.; Bird, B.; Cinque, G.; Curtis, K.; Dorney, J.; Esmonde-White, K.; Fullwood, N. J.; Gardner, B.; Martin-Hirsch, P. L.; Walsh, M. J.; McAinsh, M. R.; Stone, N.; Martin, F. L. Using Raman Spectroscopy to Characterize Biological Materials. *Nat. Protoc.* **2016**, *11* (4), 664–687. https://doi.org/10.1038/nprot.2016.036.

(7) Turunen, M.; Saarakkala, S.; Rieppo, L.; Helminen, H.; Jurvelin, J.; Isaksson, H. Raman and FTIR Spectroscopic Measurements Provide Complementary Information on Development of Bone Composition during Maturation in Rabbits. *56th Annual Meeting of the Orthopaedic Research Society*, New Orleans, LA, 2010; Poster No. 565.

(8) Ali, S. M.; Bonnier, F.; Lambkin, H.; Flynn, K.; McDonagh, V.; Healy, C.; Lee, T. C.; Lyng, F. M.; Byrne, H. J. A Comparison of Raman, FTIR and ATR-FTIR Micro Spectroscopy for Imaging Human Skin Tissue Sections. *Anal. Methods* **2013**, *5* (9), 2281–2291. https://doi.org/10.1039/c3ay40185e.

(9) Bergholt, M. S.; St-Pierre, J. P.; Offeddu, G. S.; Parmar, P. A.; Albro, M. B.; Puetzer, J. L.; Oyen, M. L.; Stevens, M. M. Raman Spectroscopy Reveals New Insights into the Zonal Organization of Native and Tissue-Engineered Articular Cartilage. *ACS Cent. Sci.* **2016**, *2* (12), 885–895. https://doi.org/10.1021/acscentsci.6b00222.

(10) Kyomoto, M.; Miwa, Y.; Pezzotti, G. Strain in UHMWPE for Orthopaedic Use Studied by Raman Microprobe Spectroscopy. *J. Biomater. Sci. Polym. Ed.* **2007**, *18* (2), 165–178. https://doi.org/10.1163/156856207779116685.

(11) Minamikawa, T.; Harada, Y.; Takamatsu, T. Ex Vivo Peripheral Nerve Detection of Rats by Spontaneous Raman Spectroscopy. *Sci. Rep.* **2015**, *5*, 1–11. https://doi.org/10.1038/srep17165.

(12) Yamamoto, T.; Minamikawa, T.; Harada, Y.; Yamaoka, Y.; Tanaka, H.; Yaku, H.; Takamatsu, T. Label-Free Evaluation of Myocardial Infarct in Surgically Excised Ventricular Myocardium by Raman Spectroscopy. *Sci. Rep.* **2018**, *8* (1), 1–10. https://doi.org/10.1038/s41598-018-33025-6.

(13) Kong, K.; Kendall, C.; Stone, N.; Notingher, I. Raman Spectroscopy for Medical Diagnostics - From in-Vitro Biofluid Assays to in-Vivo Cancer Detection. *Adv. Drug Delivery. Rev.* **2015**, *89*, 121–134. https://doi.org/10.1016/j.addr.2015.03.009.

(14) Unal, M.; Uppuganti, S.; Timur, S.; Mahadevan-Jansen, A.; Akkus, O.; Nyman, J. S. Assessing Matrix Quality by Raman Spectroscopy Helps Predict Fracture Toughness of Human Cortical Bone. *Sci. Rep.* **2019**, *9* (1), 1–13. https://doi.org/10.1038/s41598-019-43542-7.

(15) Chaichi, A.; Prasad, A.; Ranjan Gartia, M. Raman Spectroscopy and Microscopy Applications in Cardiovascular Diseases: From Molecules to Organs. *Biosensors* **2018**, *8*

(4), 1–19. https://doi.org/10.3390/bios8040107.

(16) Pezzotti, G. Raman Piezo-Spectroscopic Analysis of Natural and Synthetic Biomaterials. *Anal. Bioanal. Chem.* **2005**, *381* (3), 577–590. https://doi.org/10.1007/s00216-004-2780-1.

(17) Pezzotti, G.; Sakakura, S. Study of the Toughening Mechanisms in Bone and Biomimetic Hydroxyapatite Materials Using Raman Microprobe Spectroscopy. *J. Biomed. Mater. Res., Part A* **2003**, *65* (2), 229–236. https://doi.org/10.1002/jbm.a.10447.

(18) He, L. H.; Carter, E. A.; Swain, M. V. Characterization of Nanoindentation-Induced Residual Stresses in Human Enamel by Raman Microspectroscopy. *Anal. Bioanal. Chem.* **2007**, *389* (4), 1185–1192. https://doi.org/10.1007/s00216-007-1520-8.

(19) Finney, W. F.; Morris, M. D.; Wallace, J. M.; Kohn, D. H. Ultrastructural Elastic Deformation of Cortical Bone Tissue Probed by NIR Raman Spectroscopy. In *Biomedical Optics; San Jose, CA,* **2004***;* p.233-241. https://doi.org/10.1117/12.529456.

(20) Dooley, K. A.; McCormack, J.; Fyhrie, D. P.; Morris, M. D. Stress Mapping of Undamaged, Strained, and Failed Regions of Bone Using Raman Spectroscopy. *J. Biomed. Opt.* **2009**, *14* (4), 044018. https://doi.org/10.1117/1.3184435.

(21) Masic, A.; Bertinetti, L.; Schuetz, R.; Galvis, L.; Timofeeva, N.; Dunlop, J. W. C.; Seto, J.; Hartmann, M. A.; Fratzl, P. Observations of Multiscale, Stress-Induced Changes of Collagen Orientation in Tendon by Polarized Raman Spectroscopy. *Biomacromolecules* **2011**, *12* (11), 3989–3996. https://doi.org/10.1021/bm201008b.

(22) Chatzipanagis, K.; Baumann, C. G.; Sandri, M.; Sprio, S.; Tampieri, A.; Kröger, R. In Situ Mechanical and Molecular Investigations of Collagen/Apatite Biomimetic Composites Combining Raman Spectroscopy and Stress-Strain Analysis. *Acta Biomater.* **2016**, *46*,

278–285. https://doi.org/10.1016/j.actbio.2016.09.028.

(23) Winchester, M. W.; Winchester, L. W.; Chou, N. Y. Application of Raman Scattering to the Measurement of Ligament Tension. *Proceedings of the 30th Annual International Conference of the IEEE Engineering in Medicine and Biology Society,* Vancouver, British Columbia, CA, 2008; pp. 3434–3437. https://doi.org/10.1109/iembs.2008.4649944.

(24) Pezzotti, G.; Porporati, A. A. Raman Spectroscopic Analysis of Phase-Transformation and Stress Patterns in Zirconia Hip Joints. *J. Biomed. Opt.* **2004**, *9* (2), 372. https://doi.org/10.1117/1.1647547.

(25) Wang, P. J.; Ferralis, N.; Conway, C.; Grossman, J. C.; Edelman, E. R. Strain-Induced Accelerated Asymmetric Spatial Degradation of Polymeric Vascular Scaffolds. *Proc. Natl. Acad. Sci. U. S. A.* **2018**, *115* (11), 2640–2645. https://doi.org/10.1073/pnas.1716420115.

(26) Hwang, Y. J.; Lyubovitsky, J. G. The Structural Analysis of Three-Dimensional Fibrous Collagen Hydrogels by Raman Microspectroscopy. *Biopolymers* **2013**, *99* (6), 349–356. https://doi.org/10.1002/bip.22183.

(27) Kip, B. J.; Van Eijk, M. C. P.; Meier, R. J. Molecular Deformation of High-modulus Polyethylene Fibers Studied by Micro-raman Spectroscopy. *J. Polym. Sci., Part B: Polym. Phys.* **1991**, *29* (1), 99–108. https://doi.org/10.1002/polb.1991.090290113.

(28) Tarantili, P. A.; Andreopoulos, A. G.; Galiotis, C. Real-Time Micro-Raman Measurements on Stressed Polyethylene Fibers. 1. Strain Rate Effects and Molecular Stress Redistribution. *Macromolecules* **1998**, *31* (20), 6964–6976. https://doi.org/10.1021/ma961498l.

(29) Haston, J. L.; Engelsen, S. B.; Roessle, M.; Clarkson, J.; Blanch, E. W.; Baldock, C.;

Kielty, C. M.; Wess, T. J. Raman Microscopy and X-Ray Diffraction, a Combined Study of Fibrillin-Rich Microfibrillar Elasticity. *J. Biol. Chem.* **2003**, *278* (42), 41189–41197. https://doi.org/10.1074/jbc.M212854200.

(30) Paschou, A. M.; Katsikini, M.; Christofilos, D.; Arvanitidis, J.; Ves, S. High Pressure Raman Study of Type-I Collagen. *FEBS J.* **2018**, *285* (14), 2641–2653. https://doi.org/10.1111/febs.14506.

(31) Shao, Z.; Young, R. J.; Vollrath, F. The Effect of Solvents on Spider Silk Studied by Mechanical Testing and Single-Fibre Raman Spectroscopy. *Int. J. Biol. Macromol.* **1999**, *24* (2–3), 295–300. https://doi.org/10.1016/S0141-8130(98)00093-2.

(32) Gasior-Głogowska, M.; Komorowska, M.; Hanuza, J.; Maczka, M.; Zajac, A.; Ptak, M.; Bedziński, R.; Kobielarz, M.; Maksymowicz, K.; Kuropka, P.; Szotek, S. FT-Raman Spectroscopic Study of Human Skin Subjected to Uniaxial Stress. *J. Mech. Behav. Biomed. Mater.* **2013**, *18*, 240–252. https://doi.org/10.1016/j.jmbbm.2012.11.023.

(33) Gasior-Głogowska, M.; Komorowska, M.; Hanuza, J.; Maczka, M.; Kobielarz, M. Structural Alteration of Collagen Fibres - Spectroscopic and Mechanical Studies. *Acta Bioeng. Biomech.* **2010**, *12* (4), 53–60.

(34) Hanuza, J.; Maczka, M.; Gasior-Glogowska, M.; Komorowska, M.; Kobielarz, M.; Będziński, R.; Szotek, S.; Maksymowicz, K.; Hermanowicz, K. FT-Raman Spectroscopic Study of Thoracic Aortic Wall Subjected to Uniaxial Stress. *J. Raman Spectrosc.* **2010**, *41* (10), 1163–1169. https://doi.org/10.1002/jrs.2554.

(35) Guo, F.; Altaner, C. M. Measuring Molecular Strain in Rewetted and Never-Dried Eucalypt Wood with Raman Spectroscopy. *Biomacromolecules* **2019**, *20* (8), 3191–3199. https://doi.org/10.1021/acs.biomac.9b00808.

(36) Gierlinger, N.; Schwanninger, M.; Reinecke, A.; Burgert, I. Molecular Changes during Tensile Deformation of Single Wood Fibers Followed by Raman Microscopy. *Biomacromolecules* **2006**, *7* (7), 2077–2081. https://doi.org/10.1021/bm060236g.

(37) Lefèvre, T.; Paquet-Mercier, F.; Lesage, S.; Rousseau, M. E.; Bédard, S.; Pézolet, M. Study by Raman Spectromicroscopy of the Effect of Tensile Deformation on the Molecular Structure of Bombyx Mori Silk. *Vib. Spectrosc.* **2009**, *51* (1), 136–141. https://doi.org/10.1016/j.vibspec.2008.11.012.

(38) Sirichaisit, J.; Brookes, V. L.; Young, R. J.; Vollrath, F. Analysis of Structure/Property Relationships in Silkworm (Bombyx Mori) and Spider Dragline (Nephila Edulis) Silks Using Raman Spectroscopy. *Biomacromolecules* **2003**, *4* (2), 387–394. https://doi.org/10.1021/bm0256956.

(39) Peetla, P.; Schenzel, K. C.; Diepenbrock, W. Determination of Mechanical Strength Properties of Hemp Fibers Using Near-Infrared Fourier Transform Raman Microspectroscopy. *Appl. Spectrosc.* **2006**, *60* (6), 682–691. https://doi.org/10.1366/000370206777670602.

(40) Ghosh, D.; Subhash, G.; Orlovskaya, N. Measurement of Scratch-Induced Residual Stress within SiC Grains in ZrB2-SiC Composite Using Micro-Raman Spectroscopy. *Acta Mater.* **2008**, *56* (18), 5345–5354. https://doi.org/10.1016/j.actamat.2008.07.031.

(41) Subhash, G.; Ghosh, D.; Blaber, J.; Zheng, J. Q.; Halls, V.; Masters, K. Characterization of the 3-D Amorphized Zone beneath a Vickers Indentation in Boron Carbide Using Raman Spectroscopy. *Acta Mater.* **2013**, *61* (10), 3888–3896. https://doi.org/10.1016/j.actamat.2013.03.028.

(42) Awasthi, A.; Subhash, G. Deformation Behavior and Amorphization in Icosahedral

Boron-Rich Ceramics. *Prog. Mater. Sci.* **2020**, *112* (March), 100664. https://doi.org/10.1016/j.pmatsci.2020.100664.

(43) Awasthi, A. P.; Subhash, G. High-Pressure Deformation and Amorphization in Boron Carbide. *J. Appl. Phys.* **2019**, *125* (21), 215901. https://doi.org/10.1063/1.5091795.

(44) Parsard, G.; Subhash, G.; Jannotti, P. Amorphization-Induced Volume Change and Residual Stresses in Boron Carbide. *J. Am. Ceram. Soc.* **2018**, *101* (6), 2606–2615. https://doi.org/10.1111/jace.15417.

(45) Jannotti, P.; Subhash, G.; Zheng, J. Q.; Halls, V.; Karandikar, P. G.; Salamone, S.; Aghajanian, M. K. Raman Spectroscopic Characterization of the Core-Rim Structure in Reaction Bonded Boron Carbide Ceramics. *Appl. Phys. Lett.* **2015**, *106* (4), 041903. https://doi.org/10.1063/1.4906969.

(46) Shafiq, M.; Subhash, G. A Novel Technique for the Determination of Surface Biaxial Stress under External Confinement Using Raman Spectroscopy. *Exp. Mech.* **2014**, *54* (5), 763–774. https://doi.org/10.1007/s11340-014-9851-9.

(47) Xu, H. H. K.; Smith, D. T.; Jahanmir, S.; Romberg, E.; Kelly, J. R.; Thompson, V. P.; Rekow, E. D. Indentation Damage and Mechanical Properties of Human Enamel and Dentin. *J. Dent. Res.* **1998**, *77* (3), 472–480. https://doi.org/10.1177/00220345980770030601.

(48) Hart, N. H.; Nimphius, S.; Rantalainen, T.; Ireland, A.; Siafarikas, A.; Newton, R. U. Mechanical Basis of Bone Strength: Influence of Bone Material, Bone Structure and Muscle Action. *J. Musculoskeletal. Neuronal Interact.* **2017**, *17* (3), 114–139.

(49) Lee, A. J. C.; Ling, R. S. M.; Vangala, S. S. The Mechanical Properties of Bone Cements. *J. Med. Eng. Technol.* **1977**, *1* (3), 137–140. https://doi.org/10.3109/03091907709160626.

(50) Saha, S.; Soni, J.; Chandel, S.; Kumar, U.; Ghosh, N. Probing Intrinsic Anisotropies of Fluorescence: Mueller Matrix Approach. *J. Biomed. Opt.* **2015**, *20* (8), 085005. https://doi.org/10.1117/1.jbo.20.8.085005.

(51) Zipfel, W. R.; Williams, R. M.; Webb, W. W. Nonlinear Magic: Multiphoton Microscopy in the Biosciences. *Nat. Biotechnol.* **2003**, *21* (11), 1369–1377. https://doi.org/10.1038/nbt899.

(52) Arguello, C. A.; Rousseau, D. L.; Porto, S. P. S. First-Order Raman Effect in Wurtzite-Type Crystals. *Phys. Rev.* **1969**, *181* (3), 1351–1363. https://doi.org/10.1103/PhysRev.181.1351.

(53) Janko, M.; Davydovskaya, P.; Bauer, M.; Zink, A.; Stark, R. W. Anisotropic Raman Scattering in Collagen Bundles. *Opt. Lett.* **2010**, *35* (16), 2765. https://doi.org/10.1364/ol.35.002765.

(54) Bonifacio, A.; Sergo, V. Effects of Sample Orientation in Raman Microspectroscopy of Collagen Fibers and Their Impact on the Interpretation of the Amide III Band. *Vib. Spectrosc.* **2010**, *53* (2), 314–317. https://doi.org/10.1016/j.vibspec.2010.04.004.

(55) Van Gulick, L.; Saby, C.; Morjani, H.; Beljebbar, A. Age-Related Changes in Molecular Organization of Type I Collagen in Tendon as Probed by Polarized SHG and Raman Microspectroscopy. *Sci. Rep.* **2019**, *9* (1), 1–12. https://doi.org/10.1038/s41598-019-43636-2.

(56) Shepherd, D. V.; Shepherd, J. H.; Ghose, S.; Kew, S. J.; Cameron, R. E.; Best, S. M. The Process of EDC-NHS Cross-Linking of Reconstituted Collagen Fibres Increases Collagen Fibrillar Order and Alignment. *APL Mater.* **2015**, *3* (1), 1–13. https://doi.org/10.1063/1.4900887.

(57) Ly, E.; Piot, O.; Durlach, A.; Bernard, P.; Manfait, M. Polarized Raman Microspectroscopy Can Reveal Structural Changes of Peritumoral Dermis in Basal Cell Carcinoma. *Appl. Spectrosc.* **2008**, *62* (10), 1088–1094. https://doi.org/10.1366/000370208786049187.

(58) Unal, M.; Jung, H.; Akkus, O. Novel Raman Spectroscopic Biomarkers Indicate That Postyield Damage Denatures Bone's Collagen. *J. Bone Miner. Res.* **2016**, *31* (5), 1015–1025. https://doi.org/10.1002/jbmr.2768.

(59) Lim, N. S. J.; Hamed, Z.; Yeow, C. H.; Chan, C.; Huang, Z. Early Detection of Biomolecular Changes in Disrupted Porcine Cartilage Using Polarized Raman Spectroscopy. *J. Biomed. Opt.* **2011**, *16* (1), 017003. https://doi.org/10.1117/1.3528006.

(60) Green, E.; Ellis, R.; Winlove, P. The Molecular Structure and Physical Properties of Elastin Fibers as Revealed by Raman Microspectroscopy. *Biopolymers* **2008**, *89* (11), 931–940. https://doi.org/10.1002/bip.21037.

(61) Rousseau, M. E.; Lefèvre, T.; Beaulieu, L.; Asakura, T.; Pézolet, M. Study of Protein Conformation and Orientation in Silkworm and Spider Silk Fibers Using Raman Microspectroscopy. *Biomacromolecules* **2004**, *5* (6), 2247–2257. https://doi.org/10.1021/bm049717v.

(62) Lefèvre, T.; Rousseau, M. E.; Pézolet, M. Protein Secondary Structure and Orientation in Silk as Revealed by Raman Spectromicroscopy. *Biophys. J.* **2007**, *92* (8), 2885–2895. https://doi.org/10.1529/biophysj.106.100339.

(63) Lefèvre, T.; Rousseau, M. E.; Pézolet, M. Orientation-Insensitive Spectra for Raman Microspectroscopy. *Appl. Spectrosc.* **2006**, *60* (8), 841–846. https://doi.org/10.1366/000370206778062039.

(64) Plaza, G. R.; Pérez-Rigueiro, J.; Riekel, C.; Perea, G. B.; Agulló-Rueda, F.; Burghammer, M.; Guinea, G. V.; Elices, M. Relationship between Microstructure and Mechanical Properties in Spider Silk Fibers: Identification of Two Regimes in the Microstructural Changes. *Soft Matter* **2012**, *8* (22), 6015–6026. https://doi.org/10.1039/c2sm25446h.

(65) Rousseau, M. E.; Beaulieu, L.; Lefèvre, T.; Paradis, J.; Asakura, T.; Pézolet, M. Characterization by Raman Microspectroscopy of the Strain-Induced Conformational Transition in Fibroin Fibers from the Silkworm Samia Cynthia Ricini. *Biomacromolecules* **2006**, *7* (9), 2512–2521. https://doi.org/10.1021/bm060280w.

(66) Edwards, H. G. M.; Farwell, D. W.; Holder, J. M.; Lawson, E. E. Fourier-Transform Raman Spectroscopy of Ivory: II. Spectroscopic Analysis and Assignments. *J. Mol. Struct.* **1997**, *435* (1), 49–58. https://doi.org/10.1016/S0022-2860(97)00122-1.

(67) Frushour, B. G.; Koenig, J. L. Raman Scattering of Collagen, Gelatin, and Elastin. *Biopolymers* **1975**, *14* (2), 379–391. https://doi.org/10.1002/bip.1975.360140211.

(68) Gniadecka, M.; Nielsen, O. F.; Christensen, D. H.; Wulf, H. C. Structure of Water, Proteins, and Lipids in Intact Human Skin, Hair, and Nail. *J. Invest. Dermatol.* **1998**, *110* (4), 393–398. https://doi.org/10.1046/j.1523-1747.1998.00146.x.

(69) Sereda, V.; Lednev, I. K. Polarized Raman Spectroscopy of Aligned Insulin Fibrils. *J Raman Spectrosc* **2014**, *45* (8), 665–671. https://doi.org/10.1038/jid.2014.371.

(70) Litvinov, R. I.; Faizullin, D. A.; Zuev, Y. F.; Weisel, J. W. The α-Helix to β-Sheet Transition in Stretched and Compressed Hydrated Fibrin Clots. *Biophys. J.* **2012**, *103* (5), 1020–1027. https://doi.org/10.1016/j.bpj.2012.07.046.

(71) Fleissner, F.; Bonn, M.; Parekh, S. H. Microscale Spatial Heterogeneity of Protein Structural Transitions in Fibrin Matrices. *Sci. Adv.* **2016**, *2* (7), 1–10.

https://doi.org/10.1126/sciadv.1501778.

(72) Morris, M. D.; Finney, W. F.; Rajachar, R. M.; Kohn, D. H. Bone Tissue Ultrastructural Response to Elastic Deformation Probed by Raman Spectroscopy. *Faraday Discuss.* **2004**, *126* (1), 159–168. https://doi.org/10.1039/b304905a.

(73) Wang, Y. N.; Galiotis, C.; Bader, D. L. Determination of Molecular Changes in Soft Tissues under Strain Using Laser Raman Microscopy. *J. Biomech.* **2000**, *33* (4), 483–486. https://doi.org/10.1016/S0021-9290(99)00194-3.

(74) Ebenstein, D. M.; Park, J.; Kaplan, D. L.; Wahl, K. J. Nanomechanical and Microstructural Properties of Bombyx Mori Silk Films. *Mater. Res. Soc. Symp. Proc.* **2004**, *844*, 1–6.

(75) Sirichaisit, J.; Young, R. J.; Vollrath, F. Molecular Deformation in Spider Dragline Silk Subjected to Stress. *Polymer.* **2000**, *41* (3), 1223–1227. https://doi.org/10.1016/S0032-3861(99)00293-1.

(76) Pezzotti, G. Introducing a Unique Measurement for Biomaterial Nanomechanics. *Key Eng. Mater.* **2003**, *240–242*, 893–900. https://doi.org/10.4028/www.scientific.net/kem.240-242.893.

(77) Liu, H.; Yu, W. Study of the Structure Transformation of Wool Fibers with Raman Spectroscopy. *J. Appl. Polym. Sci.* **2007**, *103* (1), 1–7. https://doi.org/10.1002/app.23862.

(78) Colomban, R.; Colomban P. Nanomechanics of Single Keratin Fibres: A Raman Study of the α-Helix $\rightarrow$ β-Sheet Transition and the Effect of Water. *J. Raman Spectrosc.* **2007**, *38* (April), 1538–1553. https://doi.org/10.1002/jrs.

(79) Morris, M. D.; Carden, A.; Rajachar, R. M.; Kohn, D. H. Bone Microstructure Deformation Observed by Raman Microscopy. *Biomed. Diagnostic, Guid. Surg. Syst. III*

2001, *4254*, 81–89. https://doi.org/10.1117/12.427949.

(80) Bi, X.; Patil, C. A.; Lynch, C. C.; Pharr, G. M.; Mahadevan-Jansen, A.; Nyman, J. S. Raman and Mechanical Properties Correlate at Whole Bone- and Tissue-Levels in a Genetic Mouse Model. *J. Biomech.* **2011**, *44* (2), 297–303. https://doi.org/10.1016/j.jbiomech.2010.10.009.

(81) Tanaka, M.; Young, R. J. Molecular Orientation Distributions in Uniaxially Oriented Poly(L-Lactic Acid) Films Determined by Polarized Raman Spectroscopy. *Macromolecules* **2006**, *39* (9), 3312–3321. https://doi.org/10.1021/ma0526286.

(82) Raj, S.; Wojdyla, M.; Petrov, D. Studying Single Red Blood Cells Under a Tunable External Force by Combining Passive Microrheology with Raman Spectroscopy. *Cell Biochem. Biophys.* **2013**, *65* (3), 347–361. https://doi.org/10.1007/s12013-012-9439-x.

(83) Baer, A.; Horbelt, N.; Nijemeisland, M.; Garcia, S. J.; Fratzl, P.; Schmidt, S.; Mayer, G.; Harrington, M. J. Shear-Induced β-Crystallite Unfolding in Condensed Phase Nanodroplets Promotes Fiber Formation in a Biological Adhesive. *ACS Nano* **2019**, *13* (5), 4992–5001. https://doi.org/10.1021/acsnano.9b00857.

(84) Zhang, Z.; Yang, Y.; Zhou, P.; Zhang, X.; Wang, J. Effects of High Pressure Modification on Conformation and Gelation Properties of Myofibrillar Protein. *Food Chem.* **2017**, *217*, 678–686. https://doi.org/10.1016/j.foodchem.2016.09.040.

(85) Flanagan, C. D.; Unal, M.; Akkus, O.; Rimnac, C. M. Raman Spectral Markers of Collagen Denaturation and Hydration in Human Cortical Bone Tissue Are Affected by Radiation Sterilization and High Cycle Fatigue Damage. *J. Mech. Behav. Biomed. Mater.* **2017**, *75*, 314–321. https://doi.org/10.1016/j.jmbbm.2017.07.016.

(86) Du, J. Y.; Flanagan, C. D.; Bensusan, J. S.; Knusel, K. D.; Akkus, O.; Rimnac, C. M.

Raman Biomarkers Are Associated with Cyclic Fatigue Life of Human Allograft Cortical Bone. *J. Bone Jt. Surg., Am. Vol.* **2019**, *101* (17), e85(1). https://doi.org/10.2106/JBJS.18.00832.

(87) Chakraborty, N.; Wang, M.; Solocinski, J.; Kim, W.; Argento, A. Imaging of Scleral Collagen Deformation Using Combined Confocal Raman Microspectroscopy and Polarized Light Microscopy Techniques. *PLoS One* **2016**, *11* (11), 1–13. https://doi.org/10.1371/journal.pone.0165520.

(88) Timlin, J. A.; Carden, A.; Morris, M. D.; Rajachar, R. M.; Kohn, D. H. Raman Spectroscopic Imaging Markers for Fatigue-Related Microdamage in Bovine Bone. *Anal. Chem.* **2000**, *72* (10), 2229–2236. https://doi.org/10.1021/ac9913560.

(89) Mithieux, S. M.; Rasko, J. E. J.; Weiss, A. S. Synthetic Elastin Hydrogels Derived from Massive Elastic Assemblies of Self-Organized Human Protein Monomers. *Biomaterials* **2004**, *25* (20), 4921–4927. https://doi.org/10.1016/j.biomaterials.2004.01.055.

(90) Koldevitz, M. Fibrin Structure and Morphology under Shear Strain. Diploma Thesis, Max Planck Institute for Polymer Research, 2017.

(91) Colomban, P.; Dinh, H. M.; Riand, J.; Prinsloo, L. C.; Mauchamp, B. Nanomechanics of Single Silkworm and Spider Fibres: A Raman and Micro-Mechanical in Situ Study of the Conformation Change with Stress. *J. Raman Spectrosc.* **2008**, *38* (April), 1538–1553. https://doi.org/10.1002/jrs.

(92) Khmaladze, A.; Ganguly, A.; Kuo, S.; Raghavan, M.; Kainkaryam, R.; Cole, J. H.; Izumi, K.; Marcelo, C. L.; Feinberg, S. E.; Morris, M. D. Tissue-Engineered Constructs of Human Oral Mucosa Examined by Raman Spectroscopy. *Tissue Eng., Part C* **2013**, *19* (4), 299–306. https://doi.org/10.1089/ten.tec.2012.0287.

(93) Ember, K. J. I.; Hoeve, M. A.; McAughtrie, S. L.; Bergholt, M. S.; Dwyer, B. J.; Stevens, M. M.; Faulds, K.; Forbes, S. J.; Campbell, C. J. Raman Spectroscopy and Regenerative Medicine: A Review. *npj Regener. Med.* **2017**, *2*, 12. https://doi.org/10.1038/s41536-017-0014-3.

(94) Gentleman, E.; Swain, R. J.; Evans, N. D.; Boonrungsiman, S.; Jell, G.; Ball, M. D.; Shean, T. A. V.; Oyen, M. L.; Porter, A.; Stevens, M. M. Comparative Materials Differences Revealed in Engineered Bone as a Function of Cell-Specific Differentiation. *Nat. Mater.* **2009**, *8* (9), 763–770. https://doi.org/10.1038/nmat2505.

(95) Kobori, T.; Iwamoto, S.; Takeyasu, K.; Ohtani, T. Molecular Characterization of Reconstructed Skin Model by Raman Microspectroscopy: Comparison with Excised Human Skin. *Biopolymers* **2007**, *87* (4), 261–274. https://doi.org/10.1002/bip.

(96) Downing, J. M.; Ku, D. N. Effects of Frictional Losses and Pulsatile Flow on the Collapse of Stenotic Arteries. *J. Biomech. Eng.* **1997**, *119* (3), 317–324. https://doi.org/10.1115/1.2796096.

(97) Song, H. G.; Rumma, R. T.; Ozaki, C. K.; Edelman, E. R.; Chen, C. S. Vascular Tissue Engineering: Progress, Challenges, and Clinical Promise. *Cell Stem Cell* **2018**, *22* (3), 340–354. https://doi.org/10.1016/j.stem.2018.02.009.Vascular.

(98) Isenberg, B. C.; Williams, C.; Tranquillo, R. T. Small-Diameter Artificial Arteries Engineered in Vitro. *Circ. Res.* **2006**, *98* (1), 25–35. https://doi.org/10.1161/01.RES.0000196867.12470.84.

(99) Polacheck, W. J.; Chen, C. S. Measuring Cell-Generated Forces: A Guide to the Available Tools. *Nat. Methods* **2016**, *13* (5), 415–423. https://doi.org/10.1038/nmeth.3834.

(100) Smith, R.; Wright, K. L.; Ashton, L. Raman Spectroscopy: An Evolving Technique for

Live Cell Studies. *Analyst* **2016**, *141* (12), 3590–3600. https://doi.org/10.1039/c6an00152a.

(101) Ashton, L.; Hollywood, K. A.; Goodacre, R. Making Colourful Sense of Raman Images of Single Cells. *Analyst* **2015**, *140* (6), 1852–1858. https://doi.org/10.1039/c4an02298j.

(102) Cotton, T. M.; Kim, J. -H; Chumanov, G. D. Application of Surface-enhanced Raman Spectroscopy to Biological Systems. *J. Raman Spectrosc.* **1991**, *22* (12), 729–742. https://doi.org/10.1002/jrs.1250221203.

(103) Ramos, P. M.; Ruisánchez, I. Noise and Background Removal in Raman Spectra of Ancient Pigments Using Wavelet Transform. *J. Raman Spectrosc.* **2005**, *36* (9), 848–856. https://doi.org/10.1002/jrs.1370.

(104) Evans, C. L.; Potma, E. O.; Puoris'haag, M.; Côté, D.; Lin, C. P.; Xie, X. S. Chemical Imaging of Tissue in Vivo with Video-Rate Coherent Anti-Stokes Raman Scattering Microscopy. *Proc. Natl. Acad. Sci. U. S. A.* **2005**, *102* (46), 16807–16812. https://doi.org/10.1073/pnas.0508282102.

(105) Kong, K.; Rowlands, C. J.; Varma, S.; Perkins, W.; Leach, I. H.; Koloydenko, A. A.; Williams, H. C.; Notingher, I. Diagnosis of Tumors during Tissue-Conserving Surgery with Integrated Autofluorescence and Raman Scattering Microscopy. *Proc. Natl. Acad. Sci. U. S. A.* **2013**, *110* (38), 15189–15194. https://doi.org/10.1073/pnas.1311289110.

(106) Kong, K.; Zaabar, F.; Rakha, E.; Ellis, I.; Koloydenko, A.; Notingher, I. Towards Intra-Operative Diagnosis of Tumours during Breast Conserving Surgery by Selective-Sampling Raman Micro-Spectroscopy. *Phys. Med. Biol.* **2014**, *59* (20), 6141–6152. https://doi.org/10.1088/0031-9155/59/20/6141.

(107) Qi, J.; Shih, W.-C. Performance of Line-Scan Raman Microscopy for High-Throughput

Chemical Imaging of Cell Population. *Appl. Opt.* **2014**, *53* (13), 2881. https://doi.org/10.1364/ao.53.002881.

(108) Kong, L.; Zhang, P.; Setlow, P.; Li, Y. Multifocus Confocal Raman Microspectroscopy for Rapid Single-Particle Analysis. *J. Biomed. Opt.* **2011**, *16* (12), 120503. https://doi.org/10.1117/1.3662456.

(109) Kuhar, N.; Sil, S.; Verma, T.; Umapathy, S. Challenges in Application of Raman Spectroscopy to Biology and Materials. *RSC Adv.* **2018**, *8* (46), 25888–25908. https://doi.org/10.1039/c8ra04491k.

(110) Gautam, R.; Vanga, S.; Ariese, F.; Umapathy, S. Review of Multidimensional Data Processing Approaches for Raman and Infrared Spectroscopy. *EPJ Tech. Instrum.* **2015**, *2*, 8. https://doi.org/10.1140/epjti/s40485-015-0018-6.

(111) Carlomagno, C.; Banfi, P. I.; Gualerzi, A.; Picciolini, S.; Volpato, E.; Meloni, M.; Lax, A.; Colombo, E.; Ticozzi, N.; Verde, F.; Silani, V.; Bedoni, M. Human Salivary Raman Fingerprint as Biomarker for the Diagnosis of Amyotrophic Lateral Sclerosis. *Sci. Rep.* **2020**, *10* (1), 1–13. https://doi.org/10.1038/s41598-020-67138-8.

(112) Pichardo-Molina, J. L.; Frausto-Reyes, C.; Barbosa-García, O.; Huerta-Franco, R.; González-Trujillo, J. L.; Ramírez-Alvarado, C. A.; Gutiérrez-Juárez, G.; Medina-Gutiérrez, C. Raman Spectroscopy and Multivariate Analysis of Serum Samples from Breast Cancer Patients. *Lasers Med. Sci.* **2007**, *22* (4), 229–236. https://doi.org/10.1007/s10103-006-0432-8.

(113) Ichimura, T.; Chiu, L. Da; Fujita, K.; MacHiyama, H.; Yamaguchi, T.; Watanabe, T. M.; Fujita, H. Non-Label Immune Cell State Prediction Using Raman Spectroscopy. *Sci. Rep.* **2016**, *6* (November), 1–7. https://doi.org/10.1038/srep37562.

(114) Jacobs, C. C. D. and D. J. Principal Component Analysis : A Method for Determining the Essential Dynamics of Proteins. *Methods Mol Biol.* **2014**, *1084*, 193–226. https://doi.org/10.1007/978-1-62703-658-0.

(115) Chowdary, M.V.; Kumar, K. K.; Kurien, J.; Mathew, S.; Krishna, C.M. Discrimination of Normal,Benign, and Malignant Breast Tissues by Raman Spectroscopy. *Biopolymers* **2006**, *85* (4), 392–406. https://doi.org/10.1002/bip.

(116) Chan, J. W.; Taylor, D. S.; Zwerdling, T.; Lane, S. M.; Ihara, K.; Huser, T. Micro-Raman Spectroscopy Detects Individual Neoplastic and Normal Hematopoietic Cells. *Biophys. J.* **2006**, *90* (2), 648–656. https://doi.org/10.1529/biophysj.105.066761.

(117) De Gelder, J.; De Gussem, K.; Vandenabeele, P.; Moens, L. Reference Database of Raman Spectra of Biological Molecules. *J. Raman Spectrosc.* **2007**, *38* (April), 1538–1553. https://doi.org/10.1002/jrs.

(118) Movasaghi, Z.; Rehman, S.; Rehman, I. U. Raman Spectroscopy of Biological Tissues. *Appl. Spectrosc. Rev.* **2007**, *42* (5), 493–541. https://doi.org/10.1080/05704920701551530.

(119) Niaura, G. Raman Spectroscopy in Analysis of Biomolecules. *Encycl. Anal. Chem.* **2014**, 1–34. https://doi.org/10.1002/9780470027318.a0212.pub3.

(120) Swain, R. J.; Stevens, M. M. Raman Microspectroscopy for Non-Invasive Biochemical Analysis of Single Cells. *Biochem. Soc. Trans.* **2007**, *35* (3), 544–549. https://doi.org/10.1042/BST0350544.

(121) Pieters, S.; Vander Heyden, Y.; Roger, J. M.; D'Hondt, M.; Hansen, L.; Palagos, B.; De Spiegeleer, B.; Remon, J. P.; Vervaet, C.; De Beer, T. Raman Spectroscopy and Multivariate Analysis for the Rapid Discrimination between Native-like and Non-Native

States in Freeze-Dried Protein Formulations. *Eur. J. Pharm. Biopharm.* **2013**, *85* (2), 263–271. https://doi.org/10.1016/j.ejpb.2013.03.035.

(122) Evseenko, D. Articular Cartilage Disease in Noisy Raman Spectra. *J. Biophotonics* **2015**, *8* (7), 555–566. https://doi.org/10.1002/jbio.201300200.Ensemble.

(123) Morais, C. L. M.; Lima, K. M. G.; Singh, M.; Martin, F. L. Tutorial: Multivariate Classification for Vibrational Spectroscopy in Biological Samples. *Nat. Protoc.* **2020**, *15* (7), 2143–2162. https://doi.org/10.1038/s41596-020-0322-8.

(124) De Carmejane, O.; Morris, M. D.; Davis, M. K.; Stixrude, L.; Tecklenburg, M.; Rajachar, R. M.; Kohn, D. H. Bone Chemical Structure Response to Mechanical Stress Studied by High Pressure Raman Spectroscopy. *Calcif. Tissue Int.* **2005**, *76* (3), 207–213. https://doi.org/10.1007/s00223-004-0168-z.

For Table of Contents Only

Raman Spectroscopy Methods to Characterize the Mechanical Response of Soft Biomaterials

Hui Zhou, Chelsey S. Simmons, Malisa Sarntinoranont, and Ghatu Subhash[*]

Mechanical and Aerospace Engineering, University of Florida, Gainesville, Florida, 32611 USA